Observational constraints on the evolution of dust in protoplanetary disks

Martins e Oliveira, I.

7

Spectral Energy Distributions of the Young Stars with Disks in Serpens

We present the spectral energy distributions (SEDs) of the young stars surrounded by disks in the Serpens Molecular Cloud. The SEDs allow a correct separation between the stellar radiation from that re-emitted by the disks. Taking into account the distance of 415 pc, the distribution of ages is shifted to lower values, in the 1 – 3 Myr range, with a tail up to 10 Myr. The mass distribution varies between 0.2 and 1.2 $M_\odot$, with median mass of 0.7 $M_\odot$. The distribution of fractional disk luminosities resembles that of the young Taurus Molecular Cloud, with most disks consistent with passively irradiated disks. The actively accreting and non-accreting stars show very similar distributions in fractional disk luminosities, differing in the brighter tail. Comparison with a sample of Herbig Ae/Be stars shows that the T Tauri disks do not show the clear separation in fractional disk luminosities for different geometries as seen for disks around the more massive Herbig Ae/Be. Furthermore, the results for the mineralogy of the dust in the disk surface do not seem to be directly related to either stellar or disk characteristics.

Isa Oliveira, Bruno Merín, Ewine F. van Dishoeck, Klaus M. Pontoppidan

In preparation

7.1 Introduction

Protoplanetary disks are a natural consequence of the star formation process. They are created as a result of the conservation of angular momentum when a dense slowly rotating core in a molecular cloud collapses to form a star. From formation to dissipation, which takes a few million years, the disk is connected to its central star through magnetic field lines. During the evolution of the system (star+disk), material is accreted from the disk onto the star at the same time as material is blown away from the disk driven by winds and stellar radiation. For most disks, in which the central star is the main source of radiation (passive disks), the stellar radiation field defines and controls the temperature distribution throughout the disk.

There is evidence that the initial disk mass is a function of the stellar mass (Andrews & Williams 2005; Greaves & Rice 2010). In addition, different disk lifetimes have been suggested for stars of different masses, with disks around low-mass stars lasting longer (Carpenter et al. 2006; Kennedy & Kenyon 2009). If true, this evidence puts strong constraints on the number of planets, and of which type, could be formed in such disks. A great diversity in planetary systems is observed for the more than 500 exo-planets discovered to date (Udry & Santos 2007) and it is worth exploring whether the variety of planets is a consequence of the diversification in stars, and therefore their protoplanetary disks.

All these constraints point to a dependence and co-evolution of disks and their host stars. What happens to one will directly affect the other, and the best way to understand their evolution is to study them together, as a system. For this purpose, several authors have analyzed disks by studying the spectral energy distribution (SED) of the system. For young stars surrounded by disks, the SED is composed basically of the stellar radiation, which peaks at the visible/near-IR regime depending on the stellar effective temperature, and of the radiation re-processed and re-emitted by the dust in the disk. Due to the varying dust temperature with radius, the radiation emitted by the disk is concentrated in the infrared (IR) and millimeter (mm) regimes, which appears in the SED as an excess of radiation beyond that emitted by the star alone. Additionally, accretion of matter from the disk to the star is responsible for creating an excess of continuum radiation from hot gas, clearly seen in the ultra-violet (UV) regime, and strong emission lines. If the stellar characteristics are well known ($T_{\rm eff}$, $L_{\rm star}$, $M_{\rm star}$), observations of the system in different wavelength regimes will directly inform about the disk, through the SED of the system. Indeed, SEDs have been used to probe disk characteristics (e.g., geometry, mass) by a great number of authors (e.g., Meeus et al. 2001; Furlan et al. 2006; Sicilia-Aguilar et al. 2009).

During the millions of years it takes for most disks to go from their initial composition of small dust grains coupled to the gas (therefore presenting an SED with a considerable amount of IR excess) to no disk (and therefore little or no IR-excess), different processes affect the dust. Besides material accreting from the disk into the star, and material being blown away from the disk, the dust inside the disk needs to stick together and grow, if it is to form planets. Combining theory, observations

and laboratory experiments, the initial growth from dust into pebbles and boulders is fairly well understood (Weidenschilling 1980; Dominik & Tielens 1997; Blum & Wurm 2008). The further growth is still under debate, and is a very active field in simulations of planet formation. In addition to growth, a change in dust composition has been observed. Crystallization of the originally amorphous interstellar medium grains is necessary to understand the high crystallinity fraction found in many comets and interplanetary dust grains (see Wooden et al. 2007 and Pontoppidan & Brearley 2010 for recent reviews).

Furthermore, protoplanetary disks around low-mass stars are divided in two categories, separating actively accreting (classical T Tauri stars, CTTS) and non-accreting (weak-line T Tauri stars, WTTS) stars (Cieza et al. 2007). Initially it was thought that WTTS were young stars no longer surrounded by disks, with the lack of a disk being the reason that no material is accreted onto the star. It is now understood that the WTTS class comprises some systems that do not show signs of accretion even though a disk is present, in addition to stars no longer surrounded by disks (i.e. no material to accrete onto the star). By the time the gas in the disk has dissipated, possible giant planets should already have formed, leaving an optically thin disk with no IR excess. Some older stars, however, are observed to have some IR excess even though the gas has already dissipated. Those systems are called debris disks, where the presence of small dust is understood to be produced in situ, likely from collisions between large bodies.

For low-mass stars, the stellar and disk characteristics cannot be easily separated as is the case for higher mass Herbig stars (e.g. Meeus et al. 2001), unless the stellar characteristics are well known. To date, such studies have mostly concentrated on low-mass stars in the Taurus Molecular Cloud (e.g. Kenyon & Hartmann 1987, 1995). Taurus has an isolated stellar population, different from the more clustered environments of other nearby star-forming regions. Additionally, Taurus has been studied in a wide range of wavelengths, from X-rays to radio, which allows an extensive characterization of its members that are still surrounded by disks, as well as the lower fraction of young stars ($\sim$40%) around which disks have already dissipated (e.g. Padgett et al. 1999; Andrews & Williams 2005; Güdel et al. 2007). To test whether the results for the Taurus population are valid for stars in other star-forming regions (of different mean ages and environments), we have engaged in a systematic study of stars and their disks in several of the nearby low-mass star-forming regions. One of those regions is the Serpens Molecular Cloud, an actively star-forming complex containing a substantial mass of molecular gas and young stars both clustered and in isolation.

This work presents the SEDs of the young stellar population of Serpens discovered by the *Spitzer Space Telescope* legacy program "From molecular cores to planet-forming disks" (c2d, Evans et al. 2003). The stellar and disk components of these systems have been well studied (Harvey et al. 2006, 2007a,b; Oliveira et al. 2009, 2010, 2011; Spezzi et al. 2010), providing the necessary ingredients for constructing their SEDs in § 7.2. Specifically, the data are presented in § 7.2.1, the procedure to

construct the SEDs is described in § 7.2.2. From the SEDs it is possible to separate the disk from the stellar radiation, and characterize the disks. Using the new distance estimate for the cloud ($d = 415$ pc, Dzib et al. 2010), an updated distribution of ages and masses is derived in § 7.2.3. The disk characteristics are discussed in § 7.3. With stars and disks well characterized, § 7.4 investigates to what extent they affect each other. Finally, the conclusions are presented in § 7.5.

7.2 Spectral Energy Distributions

7.2.1 Data

The Serpens Molecular Cloud has been imaged by *Spitzer* as part of the c2d program. The detected sources in the IRAC and MIPS band were published by Harvey et al. (2006) and Harvey et al. (2007a), respectively. By combining the data in all bands, Harvey et al. (2007b) could identify a red population classified as young stellar object candidates, which is interpreted as being due to emission from the disk. Due to the position of Serpens in the sky, close to the galactic plane, a higher contamination is expected from red background sources, and for this reason the YSOs identified are still candidates in the sample of Harvey et al. (2007b). Confirmation of their nature as young objects members of the cloud is necessary. This can be done through spectroscopy, but can also be achieved through photometry in more bands. The final catalog of Harvey et al. (2007b) is band-merged with the Two Micron All Sky Survey (2MASS), providing data at J, H, K_s (at 1.2, 1.6 and 2.2 μm, respectively), IRAC bands 1 through 4 (at 3.6, 4.5, 5.8 and 8.0 μm) and MIPS bands 1 and 2 (at 24 and 70 μm), when available.

Oliveira et al. (2010) describe the complete, flux-limited sample of young stellar objects in Serpens that is used in this work. The 115 objects comprise the entire young IR-excess population of Serpens that is brighter than 3 mJy at 8 μm (from the catalog of Harvey et al. 2007b). Of these 115 young objects, 21 are shown to be still embedded in a dusty envelope (thus showing a rising IR spectra, often with deep ice features, as can be seen in Figure 2 of Oliveira et al. 2010). The remaining 94 objects are classified as disk sources, and are the subject of this work. Oliveira et al. (2009) derived spectral types (and therefore also temperatures) from optical spectroscopy for 62% of the Serpens flux-limited disk sample (58 objects). The remaining 36 objects are too extincted and could not be detected using 4-meter class telescopes. These objects have spectral types derived from photometry alone, which is less reliable than derivations from spectroscopy.

In addition to the optical spectroscopy and near- and mid-IR photometric data, optical R-band photometry (at 6260 Å) is available (Spezzi et al. 2010). Although these observations covered exactly the same area of Serpens that was covered by the c2d *Spitzer* observations, the high extinction toward a few directions in Serpens makes it impossible for optical detection. That means that not all objects have optical photometric data available.

Furthermore, Oliveira et al. (2010) present *Spitzer* IRS mid-IR spectroscopy (5 – 35 μm) for this sample. These spectra cover the silicate bands at 10 and 20 μm that are emitted by the dust in the surface layers of optically thick protoplanetary disks. Information about the typical sizes and composition of the emitting dust can be obtained from fitting models to these silicate bands. Those results are presented in Oliveira et al. (2011).

7.2.2 Building the SEDs

The first step to build the SED of a given object is to determine the stellar emission. For each object, a NextGen stellar photosphere (Hauschildt et al. 1999) corresponding to the spectral type of said star is selected. This model photosphere is scaled to either the optical or the 2MASS J photometric point to account for the object's brightness. The observed photometric data are corrected for extinction from its visual extinction (R_V) using the Weingartner & Draine (2001) extinction law, with R_V = 5.5. For objects without A_V values derived from the optical spectroscopy, these values are estimated by the best fit of the optical/near-IR photometry to the NextGen photosphere, on a close visual inspection of the final result SEDs.

Figure 7.1 shows the SEDs constructed for the objects in the sample. No SEDs could be constructed for objects #42 and 94 due to the lack of either optical or 2MASS near-IR photometric detections. For the other sources, Figure 7.1 shows the NextGen model photosphere (dashed black line), observed photometry (open squares), dereddened photometry (filled circles) and IRS spectrum (thick blue line). When there is no detection for the MIPS2 band at 70 μm, an upper limit is indicated by a downward arrow. A notable difference in the amounts of IR radiation in excess of the stellar photosphere is evident. This translates into a diversity of disk geometries, as inferred by mid-IR data (Oliveira et al. 2010).

Once the SEDs are built, aided by the model photosphere for each object, it is possible to separate the radiation that is being emitted by the star from that re-emitted by the disk, which was not possible by simply looking at the system emission – the integration of the radiation emitted by the system at all wavelengths gives the brightness of the entire system. By integrating the scaled NextGen model photosphere, the stellar luminosity ($L_{\rm star}$) can be directly obtained. If this value is subtracted from the emission of the entire system, the disk luminosity ($L_{\rm disk}$) can be derived. These integrations take into consideration the distance to the star, besides the fluxes at different bands.

Similar procedures for constructing SEDs are being performed for a large number of systems in most of the nearby star-forming regions observed by *Spitzer* (L. Maud private communication). In that work, all young stellar objects observed by *Spitzer* for which the central star has been optically characterized in the literature (thus providing the input $T_{\rm eff}$ needed to construct the SEDs) are considered. This large database allows comparison between the disks in Serpens with those in other star-forming regions, of different mean ages and environments. Their results for Taurus,

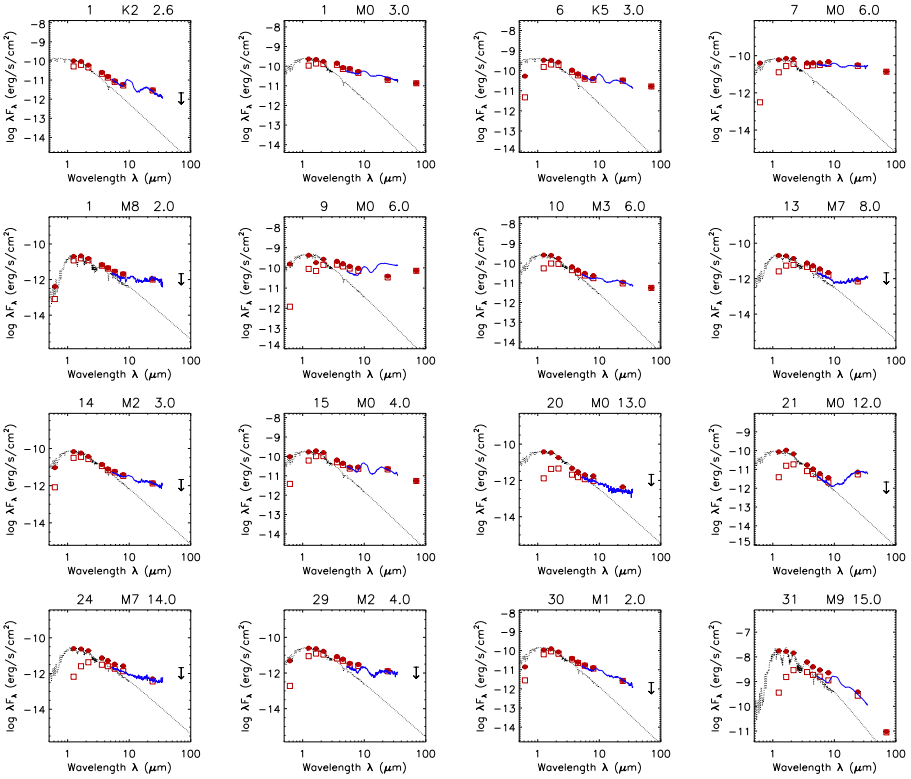

Figure 7.1 – SEDs of the young stellar population with disks of Serpens. Each SED has the corresponding object ID (as in Oliveira et al. 2010) on the top left. The solid black line indicates the NextGen stellar photosphere model for the spectral type indicated on the top of each plot. Open squares are the observed photometry while the solid circles are the dereddened photometry. The visual extinction of each object can be seen on the top right. The solid gray line is the object's IRS spectrum. Only 16 objects are shown here, the remaining 76 SEDs are shown in Appendix A.

Upper Scorpius and η Chamaeleontis will be used in this work in order to put Serpens in context.

In their derivation of stellar luminosities for the Serpens YSOs with optical spectroscopy, Oliveira et al. (2009) adopted a distance to Serpens of 259 ± 37 pc (Straizys et al. 1996, a discussion using $d = 193 \pm 13$ pc of Knude 2010 is included). However, since then the distance to the cloud has been revisited. Dzib et al. (2010) find a distance of 415 ± 15 pc to the Serpens Core from VLBA parallax observations. This new distance is used in this work. The errors in the derivation of $L_{\rm star}$ and $L_{\rm disk}$ are propagated from the errors in the distance, extinction (± 2 mag) and in the spectral type determination.

7.2.3 Masses and Ages Revisited

The new stellar luminosities, derived for the distance of 415 pc, imply that the young stars in Serpens move in the Hertzsprung-Russell (HR) diagram. The physical HR diagram relates the effective temperature ($T_{\rm eff}$) and luminosity of a star. Following Oliveira et al. (2009), $T_{\rm eff}$ is determined from the object's spectral type as follows: stars earlier than M0 follow the relationship of Kenyon & Hartmann (1995), while stars of later spectral type follow that of Luhman et al. (2003). The errors in temperature are translated directly from the errors in spectral types. With $L_{\rm star}$ and $T_{\rm eff}$ in hand, the objects can be placed in the HR diagram.

For young stellar objects, ages and masses can be derived by overlaying pre-main sequence (PMS) evolutionary tracks on the HR diagram, and comparing the position of an object to the isochrones and mass tracks, using the PMS models of Baraffe et al. (1998) and Siess et al. (2000). Due to the intrinsic physics and validation of parameters, the models of Baraffe et al. (1998) are used for stars with masses smaller than 1.4 $M_\odot$, while more massive stars are compared to the models of Siess et al. (2000). The new individual ages and masses are presented in Table A.1.

Figure 7.2 shows the distribution of masses and ages for the YSOs in Serpens. Compared to the results of Oliveira et al. (2009) for $d = 259$ pc, it is seen that the mass distribution does not change much, while the age distribution does. This is understood by looking at the isochrones and mass tracks of a given model (e.g. Figure 7 of Oliveira et al. 2009): for the temperature range of the stars in Serpens (mostly K- and M-type), mass tracks are almost vertical. This means that a change in luminosity due to the new distance hardly affects the inferred mass. From the isochrones, however, it can be noted that in general higher stellar luminosities (for this further distance) imply younger ages. Indeed, the median mass derived here is $\sim$0.7 $M_\odot$ and median age is $\sim$2.3 Myr, while Oliveira et al. (2009) found $\sim$0.7 $M_\odot$ and $\sim$5 Myr.

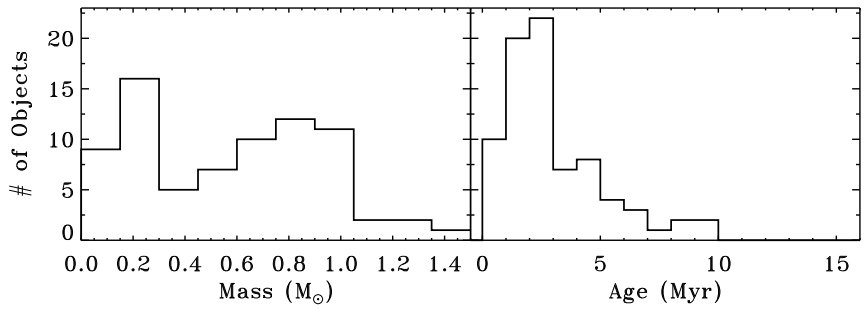

Figure 7.2 – Distribution of masses and ages of the young stellar objects in Serpens, assuming $d =$ 415 pc.

7.2.4 Notes on Individual Objects

Since the quantity of data available for each object in this sample varies, not all SEDs produce good results or yield physical parameters. Objects 31, 62, 80, 81, 86 and 103 are found to be much too luminous, which is not consistent with them being members of Serpens. The degeneracy between spectral type and extinction for sources without optical spectra makes it difficult to establish good values for both parameters. Thus, they could not be placed in the HR diagram, and therefore no ages and masses could be determined. Confirmation of their spectral type, better extinction determination, and the addition of optical photometry is necessary to revisit these objects and precisely determine their stellar parameters.

Furthermore, a few objects (# 7, 40, 48, 54, 56, 59, 60, 65, 74, 88, 101, 117 and 129) show flat SEDs. This produces large disk luminosities that deserve attention. None of these objects show signs of being (close to) edge-on. Edge-on systems will indeed produce high disk luminosities, but will also produce other signatures (e.g. inability of fitting optical/near-IR photometry to its stellar photosphere, forbidden emission lines, etc; Merín et al. 2010), which is not the case of any for the high luminosity disks shown here. Most likely, those objects are in transition from stage I (embedded) to stage II (disks) or surrounded by a nebulosity, leading to their classification as flat sources.

Lastly, object 41 seems to have a mismatch in the 2MASS photometry, making the results unreliable. For all these objects, the addition of more data will help in understanding their nature and the derivation of accurate parameters.

7.3 Disk Properties

The construction of the SEDs allows to study the diversity of disks in the same region, most of which have ages with a narrow span around a few Myr (Figure 7.2). It is clear from the SEDs that different types of disks are present in Serpens, some with lots of IR excess, others almost entirely dissipated. This is even more clear by looking at the distribution of fractional disk luminosities ($L_{\rm disk}/L_{\rm star}$) for this sample, which is presented in Figure 7.3. Here, Serpens (solid black line) is compared to the equally young, yet very different in terms of cloud structure and environment, Taurus (dotted red line, Maud et al. in prep). The peak and distribution of these two samples are very similar, with the bulk of each population showing fairly bright disks ($L_{\rm disk}/L_{\rm star} \sim 0.1$), the majority of which are consistent with passively irradiated disks ($L_{\rm disk}/L_{\rm star} \leq 0.25$, Kenyon & Hartmann 1987). This is is agreement with studies of disk geometry as inferred from IR colors, which show a large fraction of disks to be flared, based on IR colors (Oliveira et al. 2010). These two findings support the idea that these two star-forming regions are similar in spite of their different environments and star formation rate, and a good probe of the young bin of disk evolution. That is, regions in which most stars are still surrounded by disks, and most disks are flared and optically thick (at optical and IR wavelengths).

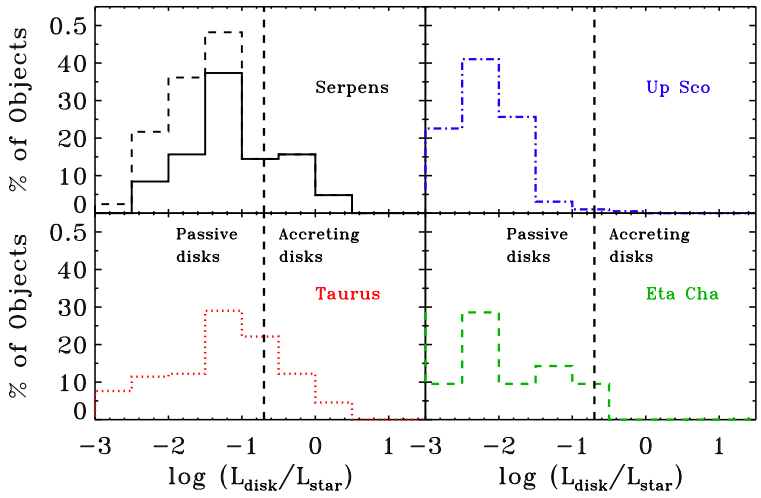

Figure 7.3 – Fractional disk luminosity ($L_{\rm disk}/L_{\rm star}$) derived for the objects in Serpens (top left), compared to those in Taurus (bottom left), Upper Scorpius (top right) and η Chamaeleontis (bottom right). The dashed line in the Serpens distribution accounts for completeness (see text for details). The boundary for accreting vs. passive disks is put at $L_{\rm disk}/L_{\rm star} \sim 0.2$. Thus "accreting disks" does not refer to the information on accretion rates derived from Hα.

Furthermore, Figure 7.3 shows the distribution of $L_{\rm disk}/L_{\rm star}$ in the Upper Scorpius and η Chamaeleontis clusters for the entire samples (consisting of objects with IR-excess and those that have little or no excess, Maud et al. in prep). These older regions are known to have lower disk fractions (Hernández et al. 2008), meaning that most of the member stars have already fully dissipated their disks. Figure 7.3 clearly shows this difference in relation to the young Serpens and Taurus clouds, with distributions that peak (and spread) at considerably lower disk luminosities. The vertical dotted lines roughly separate luminosity ratios that can be explained by different mechanisms: accretion disks ($L_{\rm disk}/L_{\rm star} > 0.2$, Kenyon & Hartmann 1987) and passive disks. "Debris"-like disks are considerably fainter ($L_{\rm disk}/L_{\rm star} < 0.001$).

It is important to note that the $L_{\rm disk}/L_{\rm star}$ distributions in Taurus, Upper Sco and η Cha are fairly complete. That is, for these well studied regions information on the entire young star population is available whether or not the source has IR excess (down to the brown dwarf limit, which ensures completeness for the results derived here for T Tauri stars). Taurus indeed has a brighter disk population than Upper Sco and η Cha. The Serpens sample presented here, on the other hand, is flux-limited and selected based on IR excess. That means that, by definition of the selection criteria, stars without disks and with disks fainter than 3 mJy at 8 μm are not part of the sample and therefore not shown in Figure 7.3. A conservative calculation of the fractional disk luminosity of the 88 missed sources (considering a flux lower than 3 mJy at 8 μm) was performed and is shown on top of the distribution of Serpens in

Figure 7.3 for reference.

Due to the selection criteria, the disk population missed in Serpens should be fainter than that presented here. Harvey et al. (2007b) identified a population of 235 IR-excess sources in Serpens, called YSO candidates. 147 of the original sample were further studied with the IRS spectrograph onboard *Spitzer*, comprising the sample presented here. This means that about 88 potential young stars with disks are missing. Considering the ∼20 % contamination fraction of background sources in the direction of Serpens (due to its low galactic latitude), conservatively about 70 of these 88 should be young stars that were missed, and which should populate the left part of Figure 7.3. These missed sources could account for the difference between Serpens and Taurus in the faintest bin of $L_{\rm disk}/L_{\rm star}$ in Figure 7.3, but should not be able to shift the peak of the $L_{\rm disk}/L_{\rm star}$ distribution for Serpens.

Serpens has not been as well explored in the literature as Taurus or Upper Sco and η Cha, since it suffers from high extinction and is not amongst the closest star-forming regions. Data covering a wide range of wavelengths exists but have not yet been published. Specifically, because this new young population in Serpens has been discovered from IR colors, young stars no longer surrounded by disks (class III) are, by definition, missed in the selection criteria for cloud membership. For this reason, the fraction of young stars that are surrounded by disks, determined for instance by combining IR and X-ray observations, is still unknown. However, the agreement in disk distribution with Taurus (as seen in Figure 7.3 and in Oliveira et al. 2010) and difference with Upper Scorpius and η Chamaeleontis could hint that the disk fraction in Serpens must be of the order of that in Taurus.

Figure 7.4 shows an additional comparison of the disks in Serpens with a sample of weak-line T Tauri stars (WTTS, Cieza et al. 2007) and a sample of debris disks (Chen et al. 2005). Oliveira et al. (2009) derived mass accretion rates based on the width at 10% of peak intensity of the Hα line, covered by their optical spectra. As previously noted, that sample is smaller than that presented here, due to the non-detection of the faintest objects in their optical spectroscopy program. It can be seen in Figure 7.4 that $L_{\rm disk}/L_{\rm star}$ of the accreting and non-accreting stars in Serpens (solid and dot-dashed black lines, respectively) overlap with the WTTSs (dotted red line). The Serpens population and the WTTSs differ in the distribution tails. The WTTS sample has a faint tail that reaches the faint debris disks population (dashed blue line), while the Serpens population shows a bright tail population.

Specifically comparing the accreting and non-accreting sub-samples in Serpens, the two classes overlap greatly, except at the brighter end of the distribution, dominated by accreting objects. This is more clearly seen by looking at the mean fractional disk luminosity $\langle L_{\rm disk}/L_{\rm star}\rangle$ which is 0.21 and 0.11 for accreting and non-accreting objects, respectively. The median fractional disk luminosity $\langle L_{\rm disk}/L_{\rm star}\rangle$ for the entire population of Serpens is 0.20.

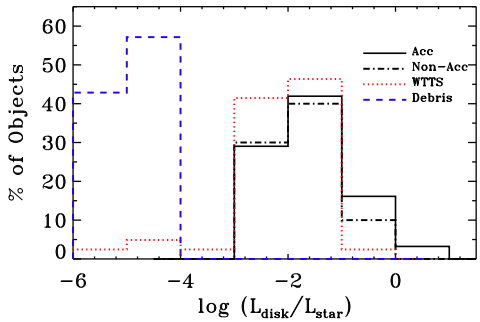

Figure 7.4 – Fractional disk luminosity ($L_{\rm disk}/L_{\rm star}$) derived for the accreting stars (based on Hα data, solid black line) and non-accreting stars (dot-dashed black line) in Serpens, compared to a sample of weak-lined T Tauri stars (WTTS, dotted gray line, Cieza et al. 2007) and a sample of debris disks (Debris, dashed gray line, Chen et al. 2005).

7.3.1 Comparison with Herbig Ae/Be Stars

Meeus et al. (2001) found that the disks around higher mass Herbig Ae/Be stars can be divided into two groups, according to the disk geometry: group I comprises sources with considerable IR excess, associated with a flared geometry; group II consists of little IR excess, associated with a geometrically thin midplane, shadowed by the puffed-up disk inner rim. Meeus et al. (2001) showed that the distributions of fractional disk luminosities for the two groups are different, with mean of 0.52 for group I and 0.17 for group II.

Figure 7.5 compares the two groups of Herbig Ae/Be stars with the young stars in Serpens, separated in disk geometry according to the ratio between the fluxes at 30 and 13 μm (F_{30}/F_{13}, Oliveira et al. 2010). It is seen that the geometry separation between flared and flat disks at $F_{30}/F_{13} = 1.5$ for T Tauri stars is not reflected with an accompanying separation in $L_{\rm disk}/L_{\rm star}$, which is the case for group I and II of the Herbig Ae/Be stars (dotted red and dashed blue lines, respectively). Although both the flared and flat disks span the same range, the peaks of the distributions are different, yielding distinctive median fractional disk luminosities: $\langle L_{\rm disk}/L_{\rm star}\rangle$ is 0.21 for the flared disks and 0.17 for flat disks.

It can be noted from Figure 7.5 that the great majority of disks around Herbig Ae/Be stars are concentrated in a narrow range of fractional disk luminosities, right at the border between disks dominated by accretion luminosity and passively irradiated disks, showing a bimodal distribution for group I and II. The T Tauri stars, on the other hand, span a much wider range of $L_{\rm disk}/L_{\rm star}$. In the center of the figure, the peaks of the distribution for flared and flat disks around T Tauri stars are not so different from those of group I and II of Herbig Ae/Be stars, albeit with greater overlap. The most striking difference between T Tauri and Herbig Ae/Be stars are both tails of the distribution. The lack of relatively very faint and very bright disks

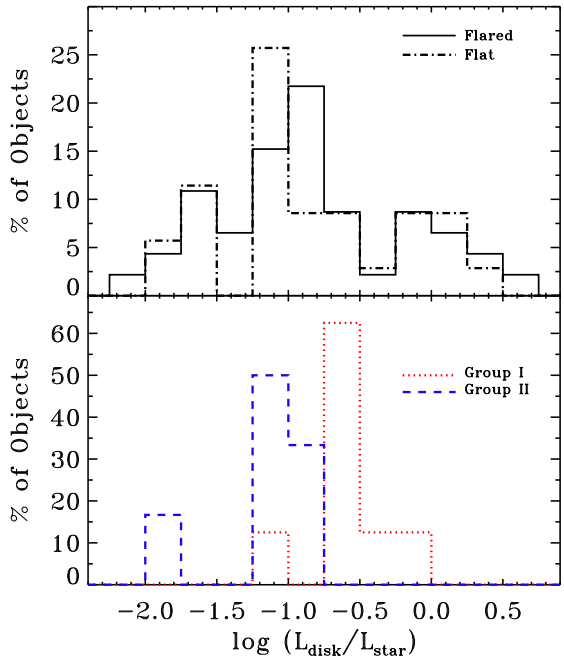

Figure 7.5 – $L_{\rm disk}/L_{\rm star}$ derived for the flared (solid black line) and flat (dot-dashed black line) disks in Serpens (top), compared to the sample of Herbig Ae/Be of Meeus et al. (2001) (bottom). Objects belonging to group I (flared, dotted gray line) and group II (self-shadowed, dashed gray line) are shown separately.

around Herbig Ae/Be stars could be a bias effect due to the considerably lower number of such disks observed, when compared to their lower mass counterparts. Another possibility is that indeed disks around higher mass stars evolve faster. That would mean that the relatively very bright phase of disk evolution happens when the disks are still embedded in a gaseous envelope and consequently not visible, while the lack of the faint end of the distribution would imply on a very fast evolution from flat disks to no disks at all, being only visible again in the debris stage.

7.4 Connection Between Stars and Disks

While the late-type (K and M) population of Serpens spans a wide variety in disk shapes, the early-type (A, F and G) stars catch the attention. Two of the 9 early-type stars (#52 and 114) are surrounded by so-called cold disks, i.e. disks depleted of warm dust close to the star but otherwise massive (Oliveira et al. 2010; Merín et al. 2010). The majority, however, show very little IR excess (#70, 80, 98, 120, 131, 139, and 145) consistent with a transition from class II to class III. Assuming the stars in

Serpens are coeval, this result supports the idea that disks around more massive stars evolve on faster timescales.

Figure 7.6 shows the stellar luminosity related to the fractional disk luminosity for the sample in Serpens (black points), Taurus (red points), Upper Sco (blue points), and η Cha (green points). Horizontal dotted lines separate stellar luminosities of Herbig Ae/Be stars (earlier than F0), T Tauri stars (down to M7) and brown dwarfs (below M7), while the vertical lines roughly separate accreting from passive disks, as in Figure 7.3. It can be seen that the few Herbig Ae stars in Serpens follow the locus of $L_{\rm disk}/L_{\rm star}$ established by the larger sample of Herbig Ae/Be stars by Meeus et al. (2001), not occupying either tail of the distribution.

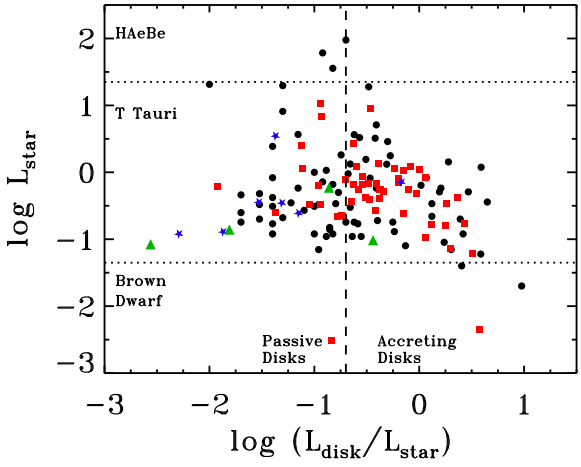

Figure 7.6 – Fractional disk luminosity ($L_{\rm disk}/L_{\rm star}$) versus the stellar luminosity ($L_{\rm star}$) derived for the objects in Serpens (black circles), compared to the objects in Taurus (gray squares), in Upper Sco (gray stars), and in η Cha (gray triangles).

Besides the stellar and disk characteristics given in § 7.2, Oliveira et al. (2011) present the dust mineralogy and mean grain sizes in the surface of disks around the stars in Serpens, together with those disks in Taurus, Upper Sco and η Cha, obtained using the exact same procedure. Those results, combined with the analysis of their SEDs by Maud et al., allow the comparison of different disk and dust characteristics for all 4 regions.

Figures 7.7, 7.8 and 7.9 relate the stellar and disk fractional luminosities and mass accretion rate, respectively, with the results from the B2C decomposition method (Olofsson et al. 2010) on the mineralogy of the dust in the upper layers of these disks. In those figures, the two upper panels show the mean mass-average grain size and the two lower panels show the mean crystallinity fraction of the dust. The two left panels are the results for the warm component close to the stars, while the right panels show the results for the cold components, further away and deeper into the disk. The low

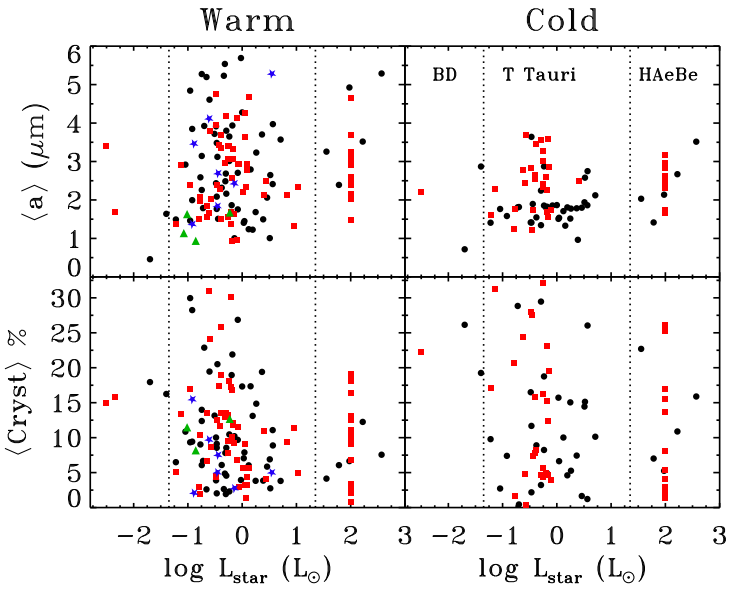

Figure 7.7 – Dust mineralogy versus the stellar luminosity ($L_{\rm star}$) derived for the objects in Serpens (black circles), compared to the objects in Taurus (gray squares), in Upper Sco (gray stars), and in η Cha (gray triangles).

number of Herbig Ae/Be stars and brown dwarfs in this sample do not allow a study across the stellar mass regime.

No strong correlations are seen in either Figures 7.7, 7.8 or 7.9, pointing to no direct cause-effect relationships between either stellar or disk fractional luminosity and the dominant grain size or crystallinity fraction of the surface dust in a disk. The results from Figure 7.8 differ from those for Herbig Ae/Be stars (Meeus et al. 2001), which find a correlation between the mean grain size in the disk surface (as derived from the silicate features) and the geometry of the disk. Their study of a small number of disks (14 objects) argues that as the disk becomes flat (transitioning from group I into group II, and therefore decreasing $L_{\rm disk}/L_{\rm star}$, as they interpret), small dust grains are removed from the disk surface (by coagulation into bigger grains or blown away by the stellar radiation), which yields larger dominating grain sizes for flatter disks. Their results are supported by a less steep sub-mm slope for group II sources than for group I. Acke et al. (2004) studied the mm slope of a sample of 26 Herbig Ae/Be stars and found a correlation between this parameter and the geometry of the disk. It is important to note, however, that the mm data probe the entire dust population and do not say anything about the size of the dust in the disk surface, as is discussed here. Acke et al. (2004) suggest a geometry evolution from flared to self-shadowed with a concurrent evolution of the size of grains in the disk. Furthermore, similar results as those of Meeus et al. (2001) are found for T Tauri stars by Bouwman

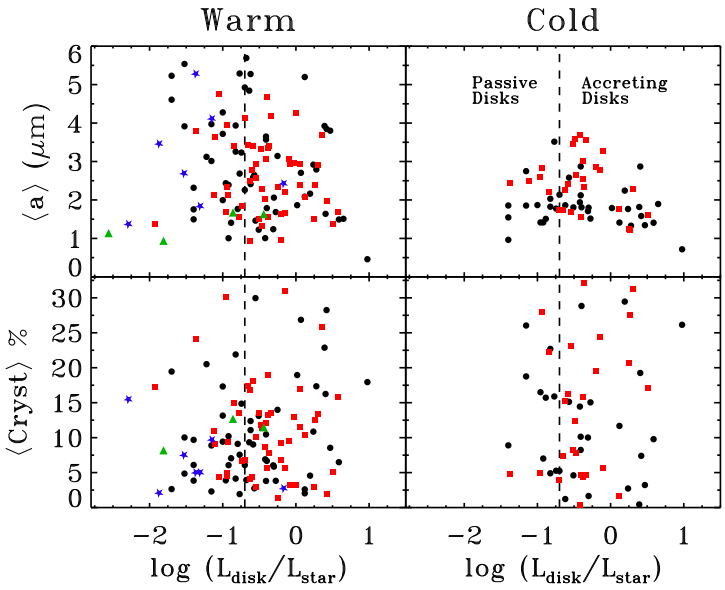

Figure 7.8 – Dust mineralogy versus the fractional disk luminosity ($L_{\rm disk}/L_{\rm star}$) derived for the objects in Serpens (black circles), compared to the objects in Taurus (gray squares), in Upper Sco (gray stars), and in η Cha (gray triangles).

et al. (2008), albeit for a very small number of objects (7 systems).

As discussed in Oliveira et al. (2010, 2011) for large samples of T Tauri stars, the dust population in the disk surface is not the result of grain growth alone, but also fragmentation of bigger grains that re-populate the small bin of grain sizes. This argument explains the presence of small grains in the disk surfaces of disks in all geometries (and even debris disks).

In addition to stellar and disk fractional luminosities and mass accretion rate, other stellar and disk parameters (such as stellar mass, disk colors and slopes) were investigated in relation to the mineralogical results. Similar to Figures 7.7, 7.8 and 7.9, no strong correlation was found for any combination of parameters. The lack of direct correlations between the stellar and disk characteristics shown above presents itself as a strong argument for the non-direct relationship of stellar and disk characteristics, in the range of parameters (time, mass, environment) probed by the objects presented here. That is, no direct causal relationship between stellar and disk characteristics is seen for T Tauri stars within a few Myr ($\sim$1 – 8 Myr). From the data presented here it is not possible to say whether any relationship could arise from studying in the same manner larger samples, that span a wider range in the parameters mentioned. Indeed, the few relationships claimed in the literature cover a large parameter space. For example, Sicilia-Aguilar et al. (2010) only found a trend of mass accretion rate decreasing over a range of dozens of millions of years, with a large spread at all ages.

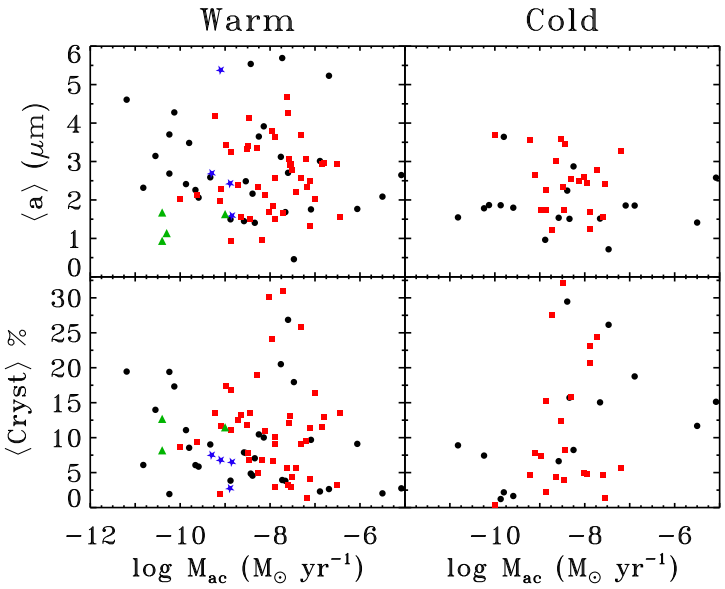

Figure 7.9 – Dust mineralogy versus the mass accretion rate of the objects in Serpens (black circles), compared to the objects in Taurus (gray squares), in Upper Sco (gray stars), and in η Cha (gray triangles).

Looking at a narrow age bin, no such relationship could be found. The same is true for the dependence of disk dispersal timescale on stellar mass found by Kennedy & Kenyon (2009). It will be interesting in the future to have a similar analysis as presented here (for stellar and disk characteristics, plus dust mineralogy) probing a wider range in stellar mass and in time, reaching the debris disk population.

7.5 Conclusions

We have studied the population of young stars still surrounded by disks in the Serpens Molecular Cloud. Aided by spectroscopic characterization of the central sources of star+disk system combined with IR photometry, spectral energy distributions of the objects could be constructed. The SEDs allow a correct separation between the radiation emitted by the central stars from that re-emitted by its surrounding disk.

The SEDs of Serpens show a considerable spread in IR excess. This implies the presence of disks with different geometries and in different stages of dissipation around stars that are nearly coeval, indicating that time is not the dominant parameter in the evolution of protoplanetary disks. The distribution of disk to star luminosity as a function of the stellar luminosity shows a trend in which lower mass stars have relatively brighter disks, consistent with evidence in the literature that disks around lower mass stars have generally longer lifetimes.

Adopting the new distance of 415 pc for Serpens, higher stellar luminosities are found than previously inferred by Oliveira et al. (2009). The higher luminosities, in turn, combined with pre-main sequence evolutionary models, allude to a distribution of ages that is younger than that found by Oliveira et al. (2009). The great majority of young stars in Serpens are in the 1 – 3 Myr range, with median age of ∼2.3 Myr. This result supports the disk observational evidence that Serpens joins the Taurus Molecular Cloud in probing the young bin of disk evolution, in spite of the different environment and star formation rates.

The distribution of fractional disk luminosity of the objects in Serpens also resembles closely that in Taurus, both of which are very different from those in the older regions Upper Scorpius and η Chamaeleontis, where most disks have already dissipated. Furthermore, the majority of the Serpens population is consistent with passively reprocessing disks. When comparing the actively accreting and non-accreting stars of Serpens (based on Hα data), the main difference seen is at the bright tail of the fractional disk luminosity, dominated by accreting stars.

The disks around T Tauri stars in Serpens are compared to those around Herbig Ae/Be stars (Meeus et al. 2001). It is found that the clear separation in fractional disk luminosity for different disk geometries (flared vs. flat) seen for Herbig Ae/Be stars is not as apparent for T Tauri stars. The disks around Herbig Ae/Be present a very narrow range of $L_{\rm disk}/L_{\rm star}$, concentrated around the border between disks dominated by accretion luminosity and passively irradiated disks, while the disks around T Tauri stars span a wider range on fractional disk luminosity. The absence of the tail distributions for Herbig Ae/Be could be due a faster evolution of these disks, or a bias effect due to the lower number of disks observed around those higher mass stars.

The stellar and disk characteristics are combined with dust mineralogy results delivered for the same regions by Oliveira et al. (2011). By combining all these data, the effect of stellar and disk characteristics on the surface dust of disks are studied. No strong correlations are found, suggesting that the many processes taking place in disks somehow conspire in such complicated ways that make it difficult to isolate the effect of each process/parameter.

References

Acke, B., van den Ancker, M. E., Dullemond, C. P., van Boekel, R., & Waters, L. B. F. M. 2004, A&A, 422, 621
Andrews, S. M., & Williams, J. P. 2005, ApJ, 631, 1134
Baraffe, I., Chabrier, G., Allard, F., & Hauschildt, P. H. 1998, A&A, 337, 403
Blum, J., & Wurm, G. 2008, ARA&A, 46, 21
Bouwman, J., et al. 2008, ApJ, 683, 479
Carpenter, J. M., Mamajek, E. E., Hillenbrand, L. A., & Meyer, M. R. 2006, ApJ, 651, L49
Chen, C. H., et al. 2005, ApJ, 634, 1372
Chiang, E. I., & Goldreich, P. 1997, ApJ, 490, 368
Cieza, L., et al. 2007, ApJ, 667, 308

Dominik, C., & Tielens, A. G. G. M. 1997, ApJ, 480, 647
Dullemond, C. P., & Dominik, C. 2004, A&A, 417, 159
Dzib, S., Loinard, L., Mioduszewski, A. J., Boden, A. F., Rodríguez, L. F., & Torres, R. M. 2010, ApJ, 718, 610
Evans, N. J., II, et al. 2003, PASP, 115, 965
Furlan, E., et al. 2006, ApJS, 165, 568
Güdel, M., et al. 2007, A&A, 468, 353
Greaves, J. S., & Rice, W. K. M. 2010, MNRAS, 407, 1981
Harvey, P. M., et al. 2006, ApJ, 644, 307
Harvey, P. M., et al. 2007, ApJ, 663, 1139
Harvey, P., Merín, B., Huard, T. L., Rebull, L. M., Chapman, N., Evans, N. J., II, & Myers, P. C. 2007, ApJ, 663, 1149
Hauschildt, P. H., Allard, F., Ferguson, J., Baron, E., & Alexander, D. R. 1999, ApJ, 525, 871
Hernández, J., Hartmann, L., Calvet, N., Jeffries, R. D., Gutermuth, R., Muzerolle, J., & Stauffer, J. 2008, ApJ, 686, 1195
Kennedy, G. M., & Kenyon, S. J. 2009, ApJ, 695, 1210
Kenyon, S. J., & Hartmann, L. 1987, ApJ, 323, 714
Kenyon, S. J., & Hartmann, L. 1995, ApJS, 101, 117
Knude, J. 2010, arXiv:1006.3676
Luhman, K. L., Stauffer, J. R., Muench, A. A., Rieke, G. H., Lada, E. A., Bouvier, J., & Lada, C. J. 2003, ApJ, 593, 1093
Maud, L. in preparation
Meeus, G., Waters, L. B. F. M., Bouwman, J., van den Ancker, M. E., Waelkens, C., & Malfait, K. 2001, A&A, 365, 476
Merín, B., et al. 2010, ApJ, 718, 1200
Oliveira, I., et al. 2009, ApJ, 691, 672
Oliveira, I., et al. 2010, ApJ, 714, 778
Oliveira, I., et al. 2011, accepted by ApJ
Olofsson, J., Augereau, J.-C., van Dishoeck, E. F., Merín, B., Grosso, N., Ménard, F., Blake, G. A., & Monin, J.-L. 2010, A&A, 520, A39
Padgett, D. L., Brandner, W., Stapelfeldt, K. R., Strom, S. E., Terebey, S., & Koerner, D. 1999, AJ, 117, 1490
Pontoppidan, K. M., & Brearley, A. J. 2010, Protoplanetary Dust: Astrophysical and Cosmochemical Perspectives, 191
Sicilia-Aguilar, A., et al. 2009, ApJ, 701, 1188
Sicilia-Aguilar, A., Henning, T., & Hartmann, L. W. 2010, ApJ, 710, 597
Siess, L., Dufour, E., & Forestini, M. 2000, A&A, 358, 593
Spezzi, L., Merin, B., Oliveira, I., van Dishoeck, E. F., & Brown, J. M. 2010, A&A, 513, A38
Straizys, V., Cernis, K. & Bartasiute, S. 1996, Baltic Astron., 5, 125
Strom, S. E., Strom, K. M., & Grasdalen, G. L. 1975, ARA&A, 13, 187
Udry, S., & Santos, N. C. 2007, ARA&A, 45, 397
Weidenschilling, S. J. 1980, Icarus, 44, 172
Weingartner, J. C., & Draine, B. T. 2001, ApJ, 548, 296
Wooden, D., Desch, S., Harker, D., Gail, H.-P., & Keller, L. 2007, Protostars and Planets V, 815

A. The Remaining SEDs

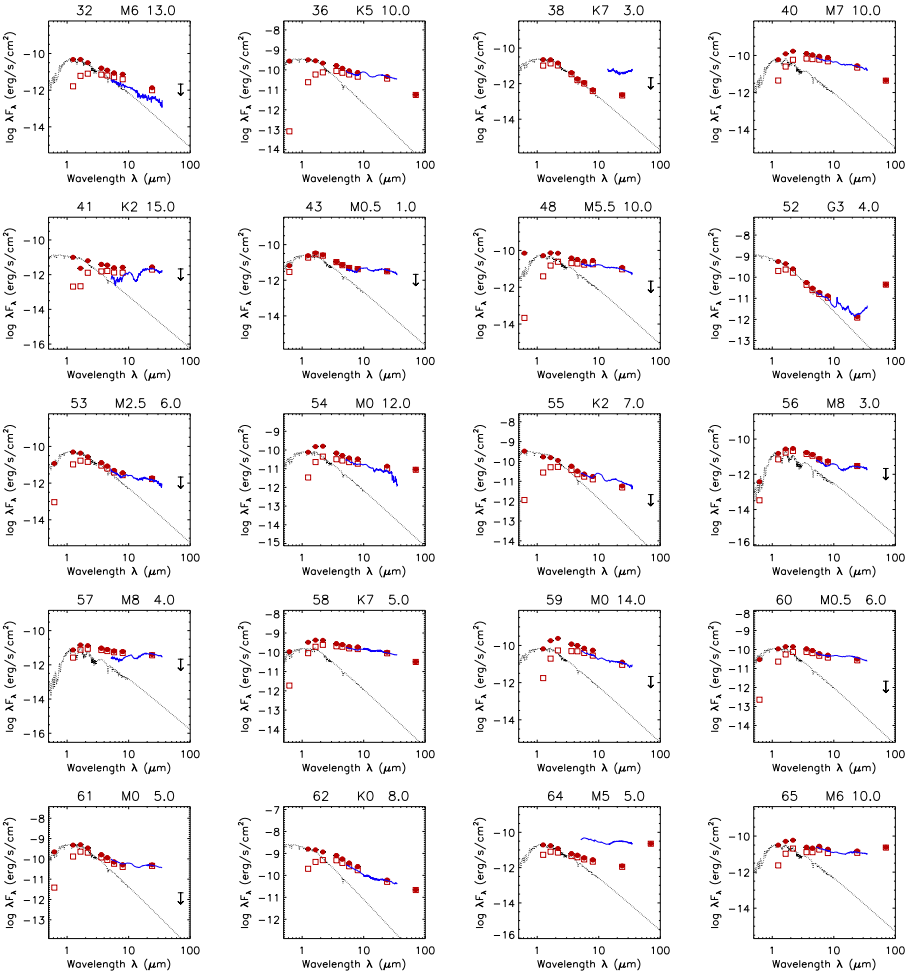

Figure A.1 – SEDs of the young stellar population with disks of Serpens. Each SED has the corresponding object ID (as in Oliveira et al. 2010) on the top left. The solid black line indicates the NextGen stellar photosphere model for the spectral type indicated on the top of each plot. Open squares are the observed photometry while the solid circles are the dereddened photometry. The visual extinction of each object can be seen on the top right. The solid gray line is the object's IRS spectrum.

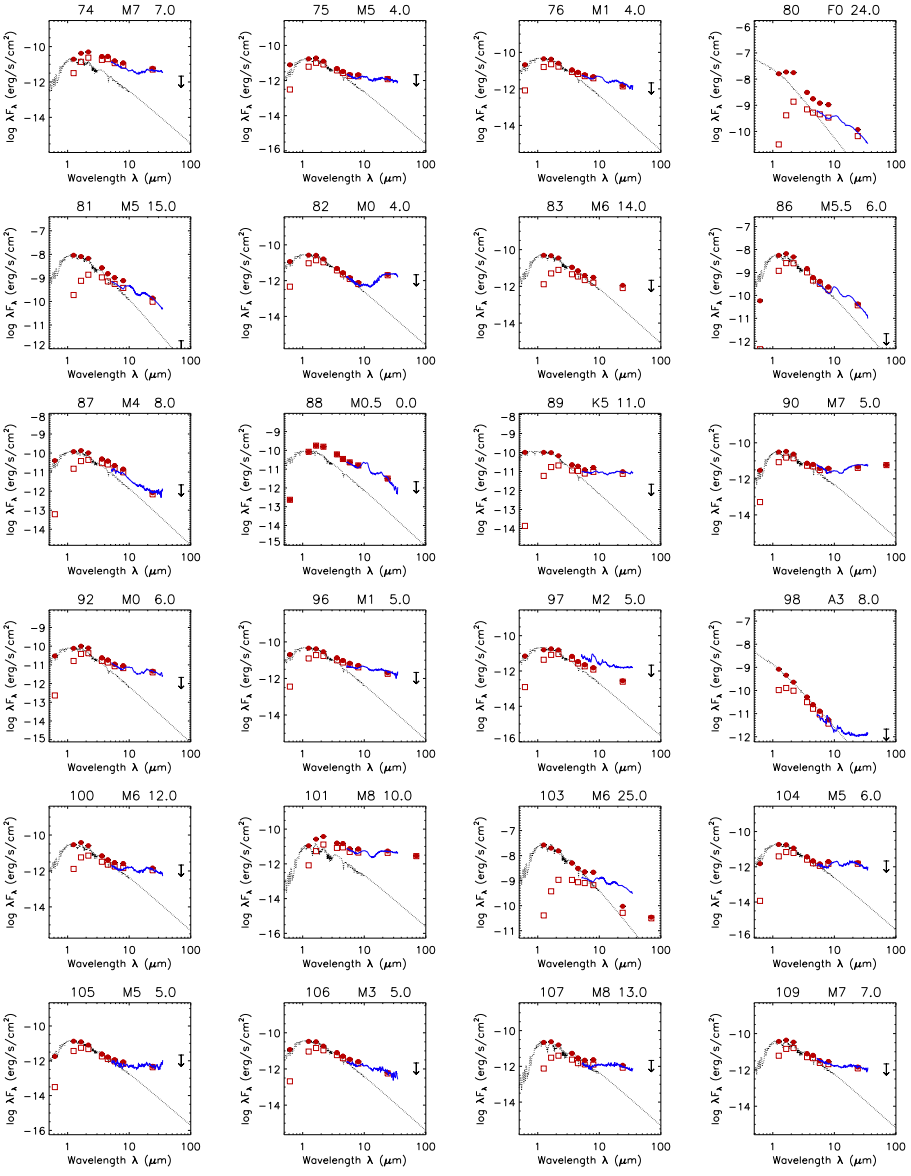

Figure A.2 – SEDs, continued.

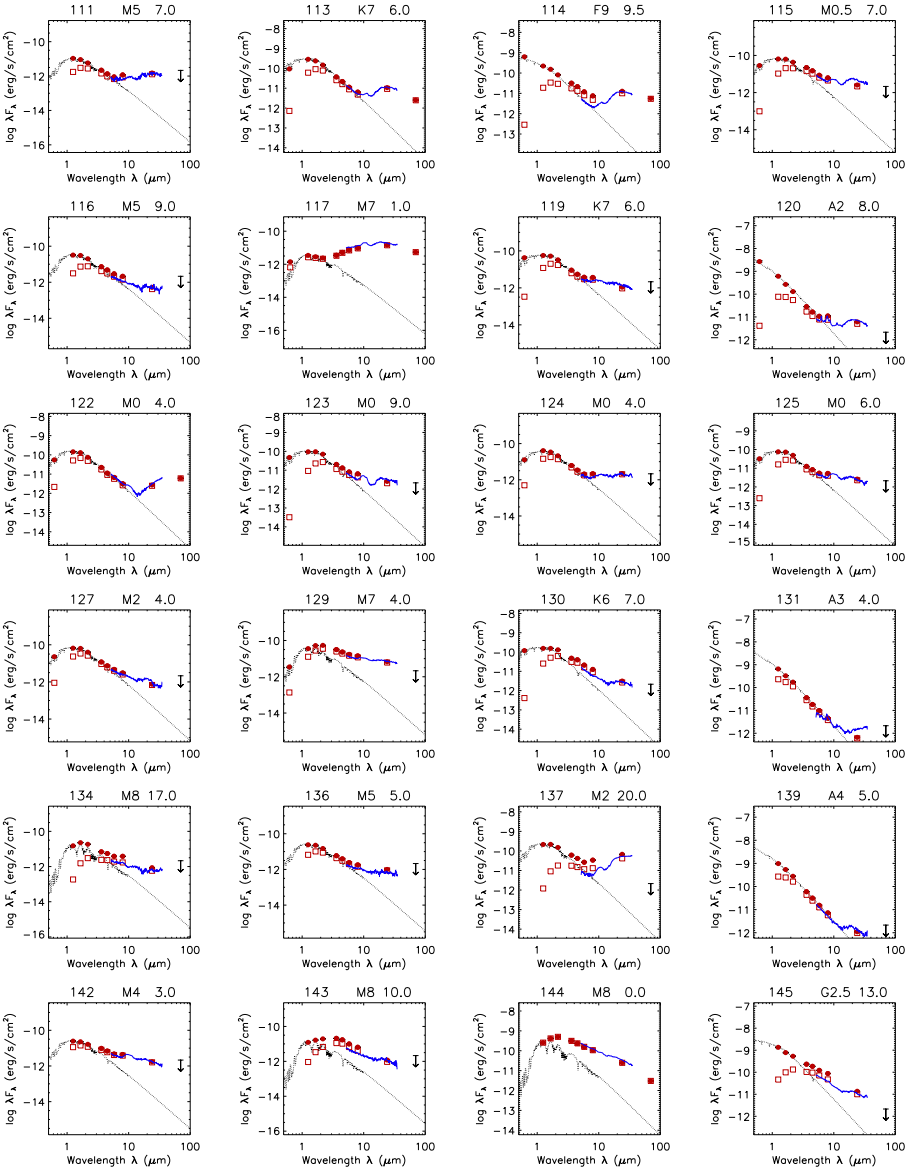

Figure A.3 – SEDs, continued.

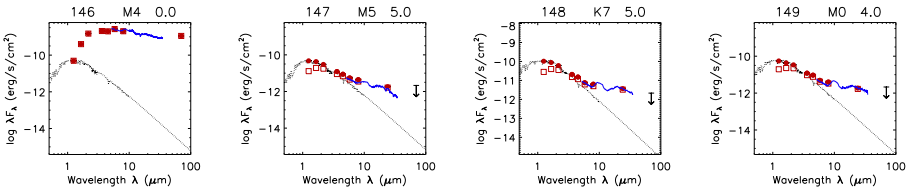

Figure A.4 – SEDs, continued.

ID[a]	SpType	T_{eff} (K)	L_{star} ($L_\odot$)	L_{disk} ($L_\odot$)	A_V	Age (Myr)	Mass ($M_\odot$)	Accr?
1	K2	4900^{+610}_{-450}	$1.07^{+0.88}_{-0.52}$	$0.13^{+0.14}_{-0.14}$	2.6	$10.86^{+16.99}_{-7.04}$	$1.27^{+0.31}_{-0.31}$	yes
3	M0	3850^{+120}_{-80}	$1.77^{+1.55}_{-0.84}$	$0.53^{+0.94}_{-0.94}$	3.0	$0.50^{+1.40}_{-0.50}$	$1.04^{+0.18}_{-0.10}$	yes
6	K5	4350^{+330}_{-340}	$3.30^{+1.79}_{-1.17}$	$0.27^{+0.89}_{-0.89}$	3.0	$2.37^{+0.30}_{-0.30}$	$1.48^{+0.27}_{-0.27}$	yes
7	M0	3850^{+120}_{-80}	$0.51^{+2.36}_{-0.42}$	$1.56^{+0.80}_{-0.80}$	6.0	$4.36^{+47.24}_{-4.36}$	$0.88^{+0.28}_{-0.24}$	yes
8[b]	M8	2640^{+450}_{-207}	$0.11^{+0.09}_{-0.05}$	$0.13^{+0.01}_{-0.01}$	2.0	$0.78^{+0.78}_{-0.78}$	$0.12^{+0.12}_{-0.12}$	–
9[b]	M0	3850^{+190}_{-220}	$3.23^{+2.82}_{-1.53}$	$0.38^{+1.22}_{-1.22}$	6.0	$0.56^{+0.56}_{-0.56}$	$1.03^{+1.03}_{-1.03}$	–
10[b]	M3	3470^{+220}_{-260}	$1.82^{+1.59}_{-0.87}$	$0.18^{+0.32}_{-0.32}$	6.0	$0.44^{+0.44}_{-0.44}$	$0.68^{+0.68}_{-0.68}$	–
13[b]	M7	2940^{+340}_{-390}	$0.12^{+0.10}_{-0.06}$	$0.15^{+0.02}_{-0.02}$	8.0	$2.54^{+2.54}_{-2.54}$	$0.24^{+0.24}_{-0.24}$	–
14	M2	3580^{+250}_{-230}	$0.49^{+0.43}_{-0.23}$	$0.00^{+0.00}_{-0.00}$	3.0	$2.27^{+3.45}_{-1.50}$	$0.63^{+0.28}_{-0.19}$	yes
15[b]	M0	3850^{+190}_{-220}	$1.32^{+1.15}_{-0.63}$	$0.49^{+0.64}_{-0.64}$	4.0	$1.01^{+1.74}_{-1.01}$	$0.98^{+0.16}_{-0.18}$	–
20[b]	M0	3850^{+190}_{-220}	$0.29^{+0.25}_{-0.14}$	$0.05^{+0.01}_{-0.00}$	13.0	$9.06^{+14.45}_{-5.16}$	$0.81^{+0.08}_{-0.25}$	–
21[b]	M0	3850^{+190}_{-220}	$0.66^{+0.58}_{-0.32}$	$0.15^{+0.10}_{-0.10}$	12.0	$2.89^{+4.58}_{-1.74}$	$0.91^{+0.14}_{-0.26}$	–
24[b]	M7	2940^{+340}_{-390}	$0.15^{+0.13}_{-0.07}$	$0.14^{+0.02}_{-0.02}$	14.0	$2.06^{+2.06}_{-2.06}$	$0.24^{+0.24}_{-0.24}$	–
29	M2	3580^{+320}_{-360}	$0.18^{+0.16}_{-0.09}$	$0.20^{+0.04}_{-0.04}$	4.0	$8.13^{+18.42}_{-6.50}$	$0.56^{+0.23}_{-0.32}$	yes
30	M1	3720^{+150}_{-120}	$1.00^{+0.53}_{-0.36}$	$0.10^{+0.10}_{-0.10}$	2.0	$1.18^{+1.13}_{-0.74}$	$0.83^{+0.18}_{-0.10}$	yes
31[b]	M9	2510^{+440}_{-107}	$94.77^{+75.01}_{-47.21}$	$0.20^{+18.94}_{-18.94}$	15.0			–
32[b]	M6	3050^{+370}_{-360}	$0.30^{+0.25}_{-0.14}$	$0.22^{+0.06}_{-0.06}$	13.0	$1.73^{+1.73}_{-1.73}$	$0.38^{+0.38}_{-0.38}$	–
36	K5	4350^{+680}_{-480}	$2.88^{+1.56}_{-1.02}$	$0.50^{+1.43}_{-1.43}$	10.0	$1.20^{+4.56}_{-1.20}$	$1.21^{+0.50}_{-0.66}$	yes
38[b]	K7	4060^{+350}_{-80}	$0.18^{+0.16}_{-0.09}$	$0.02^{+0.00}_{-0.00}$	3.0	$21.77^{+39.11}_{-13.85}$	$0.72^{+0.02}_{-0.11}$	–
40	M7	2940^{+570}_{-507}	$0.36^{+0.30}_{-0.17}$	$4.46^{+1.61}_{-1.61}$	10.0	$2.03^{+2.03}_{-2.03}$	$0.48^{+0.48}_{-0.48}$	no
41	K2	4900^{+610}_{-450}	$0.11^{+0.09}_{-0.05}$	$0.28^{+0.03}_{-0.03}$	15.0			no
43	M0.5	3785^{+225}_{-380}	$0.18^{+0.16}_{-0.09}$	$0.56^{+0.10}_{-0.10}$	1.0	$18.20^{+25.92}_{-15.10}$	$0.75^{+0.08}_{-0.37}$	no
48	M5.5	3145^{+425}_{-525}	$0.34^{+0.29}_{-0.16}$	$1.32^{+0.44}_{-0.44}$	10.0	$1.58^{+1.07}_{-1.07}$	$0.33^{+0.19}_{-0.19}$	yes
52	G3	5830^{+400}_{-230}	$8.14^{+6.40}_{-4.07}$	$0.05^{+0.43}_{-0.43}$	4.0	$6.93^{+6.33}_{-2.63}$	$1.82^{+0.39}_{-0.38}$	no
53	M2.5	3525^{+385}_{-355}	$0.35^{+0.31}_{-0.17}$	$0.06^{+0.02}_{-0.02}$	6.0	$2.34^{+6.84}_{-2.34}$	$0.50^{+0.41}_{-0.36}$	yes
54[b]	M0	3850^{+190}_{-220}	$0.58^{+0.51}_{-0.28}$	$1.61^{+0.94}_{-0.94}$	12.0	$3.44^{+5.18}_{-1.97}$	$0.90^{+0.14}_{-0.26}$	–
55	K2	4900^{+450}_{-210}	$2.44^{+10.94}_{-2.03}$	$0.04^{+0.09}_{-0.09}$	7.0	$4.02^{+36.50}_{-4.02}$	$1.68^{+1.13}_{-0.80}$	yes
56[b]	M8	2640^{+450}_{-207}	$0.09^{+0.07}_{-0.04}$	$1.73^{+0.15}_{-0.15}$	3.0	$1.27^{+1.27}_{-1.27}$	$0.12^{+0.12}_{-0.12}$	–
57[b]	M8	2640^{+450}_{-207}	$0.04^{+0.03}_{-0.02}$	$2.54^{+0.11}_{-0.11}$	4.0	$2.94^{+2.94}_{-2.94}$	$0.11^{+0.11}_{-0.11}$	–
58	K7	4060^{+350}_{-80}	$1.19^{+5.48}_{-0.98}$	$3.89^{+4.62}_{-4.62}$	5.0	$2.31^{+24.92}_{-2.31}$	$1.14^{+0.25}_{-0.14}$	yes
59[b]	M0	3850^{+190}_{-220}	$0.51^{+0.44}_{-0.24}$	$2.94^{+1.49}_{-1.49}$	14.0	$4.42^{+5.41}_{-2.58}$	$0.87^{+0.14}_{-0.26}$	–
60	M0.5	3785^{+50}_{-80}	$0.83^{+0.73}_{-0.40}$	$1.17^{+0.97}_{-0.97}$	6.0	$2.20^{+3.35}_{-1.51}$	$0.93^{+0.08}_{-0.10}$	yes
61	M0	3850^{+120}_{-80}	$3.65^{+3.19}_{-1.73}$	$0.24^{+0.87}_{-0.87}$	5.0	$0.40^{+0.40}_{-0.40}$	$1.05^{+1.05}_{-1.05}$	yes
62	K0	5250^{+630}_{-1140}	$18.94^{+15.34}_{-9.34}$	$0.33^{+6.16}_{-6.16}$	8.0			no
64[b]	M5	3240^{+270}_{-260}	$0.13^{+0.11}_{-0.06}$	$0.58^{+0.08}_{-0.08}$	5.0	$2.05^{+5.19}_{-2.05}$	$0.21^{+0.21}_{-0.11}$	–
65[b]	M6	3050^{+370}_{-360}	$0.20^{+0.17}_{-0.10}$	$2.46^{+0.49}_{-0.49}$	10.0	$1.48^{+1.11}_{-1.11}$	$0.23^{+0.12}_{-0.12}$	–
66	K5	4350^{+330}_{-340}	$5.11^{+4.35}_{-2.46}$	$0.39^{+1.99}_{-1.99}$	7.0	$1.64^{+0.17}_{-0.17}$	$1.56^{+0.35}_{-0.35}$	yes
69[b]	M5	3240^{+270}_{-260}	$0.23^{+0.20}_{-0.11}$	$0.00^{+0.00}_{-0.00}$	11.0	$0.77^{+2.22}_{-0.77}$	$0.21^{+0.23}_{-0.07}$	–
70	A3	8720^{+720}_{-775}	$20.64^{+15.11}_{-10.63}$	$0.01^{+0.22}_{-0.22}$	3.0	$8.18^{+70.19}_{-8.18}$	$2.10^{+0.38}_{-0.21}$	no
71	M3	3470^{+80}_{-130}	$0.33^{+0.29}_{-0.16}$	$0.03^{+0.01}_{-0.01}$	4.0	$2.48^{+3.15}_{-1.37}$	$0.49^{+0.09}_{-0.11}$	yes
74[b]	M7	2940^{+340}_{-390}	$0.12^{+0.10}_{-0.06}$	$2.62^{+0.31}_{-0.31}$	7.0	$2.66^{+2.66}_{-2.66}$	$0.24^{+0.24}_{-0.24}$	–
75[b]	M5	3240^{+270}_{-260}	$0.11^{+0.10}_{-0.05}$	$0.23^{+0.03}_{-0.03}$	4.0	$2.33^{+5.95}_{-2.33}$	$0.21^{+0.21}_{-0.11}$	–
76	M1	3720^{+150}_{-120}	$0.33^{+0.29}_{-0.16}$	$0.11^{+0.04}_{-0.04}$	4.0	$5.66^{+7.09}_{-3.29}$	$0.71^{+0.16}_{-0.14}$	no
80[b]	F0	7200^{+380}_{-310}	$370.99^{+288.34}_{-86.29}$	$0.17^{+62.16}_{-62.16}$	24.0			–
81	M5	3240^{+520}_{-690}	$60.77^{+52.31}_{-29.09}$	$0.12^{+7.38}_{-7.38}$	15.0			–
82	M0	3850^{+190}_{-220}	$0.20^{+0.18}_{-0.10}$	$0.03^{+0.01}_{-0.01}$	4.0	$15.80^{+21.23}_{-9.13}$	$0.76^{+0.08}_{-0.22}$	yes
83[b]	M6	3050^{+370}_{-360}	$0.31^{+0.26}_{-0.15}$	$0.04^{+0.01}_{-0.01}$	14.0	$1.64^{+1.64}_{-1.64}$	$0.38^{+0.38}_{-0.38}$	–
86	M5.5	3145^{+270}_{-160}	$35.78^{+30.57}_{-17.19}$	$0.15^{+5.50}_{-5.50}$	6.0			–
87	M4	3370^{+320}_{-460}	$0.82^{+0.72}_{-0.39}$	$0.34^{+0.28}_{-0.28}$	8.0	$1.43^{+0.24}_{-0.24}$	$0.64^{+0.19}_{-0.19}$	no
88	M0.5	3785^{+155}_{-275}	$0.64^{+0.56}_{-0.31}$	$1.04^{+0.67}_{-0.67}$	0.0	$2.98^{+4.76}_{-1.80}$	$0.91^{+0.12}_{-0.30}$	no
89	K5	4350^{+850}_{-550}	$0.95^{+0.81}_{-0.46}$	$0.21^{+0.20}_{-0.20}$	11.0	$5.11^{+21.66}_{-3.76}$	$1.18^{+0.02}_{-0.62}$	yes
90[b]	M7	2940^{+680}_{-507}	$0.19^{+0.16}_{-0.09}$	$0.40^{+0.08}_{-0.08}$	5.0	$7.34^{+7.34}_{-7.34}$	$0.54^{+0.54}_{-0.54}$	–
92	M0	3850^{+120}_{-80}	$0.58^{+0.51}_{-0.28}$	$0.39^{+0.23}_{-0.23}$	6.0	$3.40^{+5.17}_{-1.95}$	$0.90^{+0.10}_{-0.10}$	yes
96	M1	3720^{+150}_{-120}	$0.34^{+0.30}_{-0.16}$	$0.16^{+0.06}_{-0.06}$	5.0	$5.51^{+6.80}_{-3.19}$	$0.72^{+0.16}_{-0.14}$	yes
97	M2	3580^{+250}_{-230}	$0.14^{+0.08}_{-0.05}$	$0.14^{+0.02}_{-0.02}$	5.0	$10.11^{+18.68}_{-6.67}$	$0.55^{+0.19}_{-0.22}$	no
98	A3	8720^{+3100}_{-1220}	$32.48^{+23.78}_{-16.72}$	$0.00^{+0.12}_{-0.12}$	8.0	$4.99^{+7.78}_{-1.68}$	$2.42^{+0.45}_{-0.44}$	no
100[b]	M6	3050^{+370}_{-360}	$0.18^{+0.15}_{-0.09}$	$0.24^{+0.04}_{-0.04}$	12.0	$1.61^{+1.15}_{-1.15}$	$0.22^{+0.12}_{-0.12}$	–

ID[a]	SpType	T_{eff} (K)	L_{star} ($L_\odot$)	L_{disk} ($L_\odot$)	A_V	Age (Myr)	Mass ($M_\odot$)	Accr?
101[b]	M8	2640^{+450}_{-207}	$0.06^{+0.05}_{-0.03}$	$3.86^{+0.24}_{-0.24}$	10.0	$2.02^{+2.02}_{-2.02}$	$0.12^{+0.12}_{-0.12}$	–
103[b]	M6	3050^{+370}_{-360}	$166.68^{+141.01}_{-80.49}$	$0.06^{+0.69}_{-0.00}$	25.0			–
104[b]	M5	3240^{+270}_{-260}	$0.12^{+0.11}_{-0.06}$	$0.10^{+0.01}_{-0.01}$	6.0	$2.16^{+5.49}_{-2.16}$	$0.21^{+0.21}_{-0.11}$	–
105[b]	M5	3240^{+270}_{-260}	$0.09^{+0.05}_{-0.03}$	$0.00^{+0.00}_{-0.00}$	5.0	$2.91^{+7.96}_{-2.91}$	$0.21^{+0.20}_{-0.12}$	–
106	M3	3470^{+80}_{-130}	$0.25^{+0.13}_{-0.09}$	$0.02^{+0.01}_{-0.01}$	5.0	$3.10^{+3.20}_{-1.02}$	$0.47^{+0.08}_{-0.11}$	no
107[b]	M8	2640^{+450}_{-207}	$0.12^{+0.10}_{-0.06}$	$0.04^{+0.01}_{-0.01}$	13.0	$0.63^{+0.63}_{-0.63}$	$0.12^{+0.12}_{-0.12}$	–
109[b]	M7	2940^{+340}_{-390}	$0.22^{+0.19}_{-0.11}$	$0.19^{+0.04}_{-0.04}$	7.0	$1.16^{+1.16}_{-1.16}$	$0.25^{+0.25}_{-0.25}$	–
111[b]	M5	3240^{+270}_{-260}	$0.07^{+0.04}_{-0.02}$	$0.11^{+0.01}_{-0.01}$	7.0	$4.26^{+13.41}_{-4.26}$	$0.20^{+0.20}_{-0.11}$	–
113	K7	4060^{+350}_{-80}	$2.32^{+2.02}_{-1.11}$	$0.03^{+0.08}_{-0.00}$	6.0	$0.68^{+1.66}_{-0.13}$	$0.13^{+0.91}_{-0.22}$	yes
114	F9	6115^{+390}_{-400}	$3.68^{+2.87}_{-1.84}$	$0.07^{+0.24}_{-0.24}$	9.5	$14.29^{+17.38}_{-14.15}$	$116.38^{+1.39}_{-0.18}$	no
115	M0.5	3785^{+155}_{-275}	$0.50^{+0.43}_{-0.24}$	$0.17^{+0.09}_{-0.09}$	7.0	$4.58^{+5.47}_{-2.84}$	$0.87^{+0.12}_{-0.31}$	no
116[b]	M5	3240^{+270}_{-260}	$0.21^{+0.18}_{-0.10}$	$0.05^{+0.01}_{-0.01}$	9.0	$0.93^{+2.29}_{-0.93}$	$0.21^{+0.22}_{-0.08}$	–
117[b]	M7	2940^{+680}_{-507}	$0.02^{+0.02}_{-0.01}$	$9.47^{+0.20}_{-0.20}$	1.0	$3.14^{+4.07}_{-3.14}$	$0.06^{+0.73}_{-0.00}$	yes
119	K7	4060^{+350}_{-80}	$0.46^{+0.40}_{-0.22}$	$0.02^{+0.01}_{-0.01}$	6.0	$4.86^{+9.08}_{-2.33}$	$0.73^{+0.27}_{-0.09}$	yes
120	A2	8970^{+520}_{-540}	$25.13^{+18.67}_{-12.86}$	$0.00^{+0.06}_{-0.00}$	8.0	$6.69^{+2.10}_{-6.69}$	$2.24^{+0.35}_{-0.29}$	no
122	M0	3850^{+155}_{-150}	$1.10^{+0.96}_{-0.52}$	$0.03^{+0.03}_{-0.00}$	4.0	$1.43^{+2.03}_{-1.12}$	$0.96^{+0.15}_{-0.16}$	yes
123	M0	3850^{+120}_{-80}	$0.72^{+0.63}_{-0.34}$	$0.12^{+0.09}_{-0.09}$	9.0	$2.63^{+4.10}_{-1.66}$	$0.92^{+0.12}_{-0.10}$	no
124	M0	3850^{+155}_{-150}	$0.27^{+0.15}_{-0.10}$	$0.08^{+0.02}_{-0.02}$	4.0	$9.68^{+10.12}_{-3.71}$	$0.81^{+0.06}_{-0.17}$	no
125	M0	3850^{+120}_{-80}	$0.58^{+0.51}_{-0.28}$	$0.07^{+0.04}_{-0.04}$	6.0	$3.45^{+5.18}_{-1.98}$	$0.90^{+0.10}_{-0.10}$	yes
127	M2	3580^{+120}_{-130}	$0.48^{+0.42}_{-0.23}$	$0.03^{+0.02}_{-0.02}$	4.0	$2.35^{+3.15}_{-1.46}$	$0.63^{+0.15}_{-0.12}$	yes
129[b]	M7	2940^{+340}_{-390}	$0.22^{+0.18}_{-0.11}$	$1.32^{+0.29}_{-0.29}$	4.0	$1.23^{+1.23}_{-1.23}$	$0.25^{+0.25}_{-0.25}$	–
130	K6	4205^{+150}_{-140}	$1.33^{+1.15}_{-0.64}$	$0.22^{+0.30}_{-0.30}$	7.0	$2.16^{+2.43}_{-2.16}$	$0.91^{+0.22}_{-0.16}$	yes
131	A3	8720^{+720}_{-775}	$25.57^{+18.72}_{-13.16}$	$0.00^{+0.02}_{-0.02}$	4.0	$6.49^{+2.08}_{-6.49}$	$2.23^{+0.37}_{-0.30}$	no
134[b]	M8	2640^{+450}_{-207}	$0.08^{+0.07}_{-0.04}$	$0.74^{+0.06}_{-0.06}$	17.0	$1.30^{+1.30}_{-1.30}$	$0.12^{+0.12}_{-0.12}$	–
136[b]	M5	3240^{+270}_{-260}	$0.17^{+0.09}_{-0.06}$	$0.04^{+0.01}_{-0.01}$	5.0	$1.44^{+3.61}_{-1.44}$	$0.21^{+0.22}_{-0.10}$	–
137[b]	M2	3580^{+250}_{-230}	$1.56^{+1.36}_{-0.74}$	$0.31^{+0.48}_{-0.48}$	20.0	$1.01^{+0.06}_{-0.06}$	$0.89^{+0.18}_{-0.18}$	–
139	A4	8460^{+1120}_{-820}	$33.71^{+24.87}_{-17.30}$	$0.00^{+0.14}_{-0.14}$	5.0	$4.77^{+4.60}_{-1.79}$	$2.43^{+0.39}_{-0.45}$	no
142	M4	3370^{+180}_{-350}	$0.17^{+0.09}_{-0.06}$	$0.26^{+0.05}_{-0.05}$	3.0	$3.05^{+4.84}_{-3.05}$	$0.36^{+0.18}_{-0.23}$	yes
143[b]	M8	2640^{+450}_{-207}	$0.07^{+0.06}_{-0.03}$	$2.02^{+0.14}_{-0.14}$	10.0	$1.76^{+1.76}_{-1.76}$	$0.12^{+0.12}_{-0.12}$	–
144[b]	M8	2640^{+450}_{-207}	$1.43^{+1.16}_{-0.70}$	$1.90^{+2.71}_{-2.71}$	0.0			–
145	G2.5	5845^{+230}_{-30}	$19.73^{+15.51}_{-9.86}$	$0.05^{+1.01}_{-1.01}$	13.0	$3.19^{+2.66}_{-0.89}$	$2.47^{+0.44}_{-0.52}$	no
146	M4	3370^{+180}_{-350}	$0.34^{+0.30}_{-0.16}$	$89.13^{+30.44}_{-30.44}$	0.0	$1.65^{+1.39}_{-1.65}$	$0.42^{+0.16}_{-0.26}$	yes
147[b]	M5	3240^{+270}_{-260}	$0.31^{+0.27}_{-0.15}$	$0.10^{+0.03}_{-0.03}$	5.0	$0.37^{+1.98}_{-0.37}$	$0.20^{+0.26}_{-0.05}$	–
148	K7	4060^{+350}_{-80}	$0.83^{+0.72}_{-0.40}$	$0.04^{+0.03}_{-0.03}$	5.0	$2.58^{+2.87}_{-1.48}$	$0.70^{+0.42}_{-0.08}$	yes
149	M0	3850^{+190}_{-220}	$0.42^{+0.37}_{-0.20}$	$0.04^{+0.02}_{-0.02}$	4.0	$5.82^{+7.72}_{-3.47}$	$0.85^{+0.14}_{-0.26}$	yes

Table A.1 – Stellar and Disk Parameters in Serpens

[a] As in Oliveira et al. (2010).
[b] Spectral types from photometry.